Palaeogeography, Palaeoclimatology, Palaeoecology 646 (2024) 112216

Contents lists available at ScienceDirect

Palaeogeography, Palaeoclimatology, Palaeoecology

journal homepage: www.elsevier.com/locate/palaeo

# Low-salinity conditions in the "marine" Late Triassic-Early Jurassic Neuquén Basin of Argentina: Challenges in paleosalinity interpretation

Mariano N. Remírez [a,*], Thomas J. Algeo [b,c,d], Jun Shen [b], Jinhua Liu [b], Geoffrey J. Gilleaudeau [a], Lian Zhou [b]

[a] Department of Atmospheric, Oceanic and Earth Sciences, George Mason University, Fairfax, 4400 University Dr, Virginia 22032, USA
[b] State Key Laboratory of Geological Processes and Mineral Resources, China University of Geosciences, Wuhan, Hubei 430074, PR China
[c] State Key Laboratory of Biogeology and Environmental Geology, China University of Geosciences, Wuhan, Hubei 430074, PR China
[d] Department of Geosciences, University of Cincinnati, OH 45221-0013, Cincinnati, USA

ARTICLE INFO

**Editor:** Bing Shen

*Keywords:*
Boron
B/Ga
Sr/Ba
Freshwater
Brackish
Arroyo Malo

ABSTRACT

Salinity, a key property of watermasses, is difficult to reconstruct in paleodepositional systems, and errors in assigning salinity facies to epicratonic and marginal-marine deposits may be common. In this study, we evaluate the salinity conditions of mudstones of the Arroyo Malo Formation (AMF), spanning the Triassic-Jurassic transition (TJT) of the Neuquén Basin, Argentina. Although the AMF has long been considered marine based on its fossil fauna, we find that three elemental salinity proxies (B/Ga, Sr/Ba, S/TOC) are consistent in indicating dominantly freshwater influence, with occasional excursions to low-brackish conditions. In this context, the sparse, fragmented, and poorly preserved assemblage of bioclasts in the AMF do not accurately represent its salinity facies. We infer that, during the TJT, the Neuquén Basin was largely isolated from the Panthalassic Ocean, or perhaps intermittently weakly connected to it. The same elemental salinity proxies indicate low-brackish conditions in a Lower Jurassic unit previously assumed to be marine and fully marine conditions in Lower Cretaceous mudstone formations of the Neuquén Basin. This trend documents the gradual establishment of open communication with the Panthalassic Ocean, with fully marine conditions prevailing by the Middle to Late Jurassic. Standard redox proxies show that the AMF watermass was not markedly reducing, demonstrating that the impoverishment of the fossil biota was not due to unfavorable redox conditions. These findings demonstrate that inferences of marine conditions based on fossil content are potentially erroneous, and they emphasize the general need to make use of salinity proxies in analysis of deep-time depositional systems.

## 1. Introduction

Salinity is one of the most important properties of a watermass, controlling its density in concert with temperature and strongly influencing water-column stratification and biocommunity composition. Evaluation of paleosalinity is essential in marginal-marine and cratonic-interior settings in which seawater and freshwater meet and mix in variable proportions (Bhattacharya, 1978). Many salinity proxies have been developed (e.g., stable isotopes, Anderson and Arthur, 1983) but few can be applied to bulk sediment. As a result, the assessment of environmental salinity conditions from the past has increasingly relied upon the examination of fossils, even with the biases that this approach can present (Fürsich, 1994). Recently, however, a set of elemental proxies consisting of boron/gallium (B/Ga), strontium/barium (Sr/Ba), and sulfur/total organic carbon (S/TOC) was developed for analysis of paleosalinity in mudstone and shale formations (Wei and Algeo, 2020), and these proxies are beginning to rewrite the history of salinity conditions in many epicratonic watermasses (Remírez and Algeo, 2020; Cheng et al., 2021; Song et al., 2021; Wei et al., 2022; Gilleaudeau et al., 2023; Liu et al., 2024).

Interpretation of paleoenvironmental conditions such as salinity in ancient epeiric seas is constrained by a dearth of modern analogues. Modern epeiric seas show considerable variation in watermass salinity as a function of regional climate. The Baltic Sea, located in a humid climate belt, exhibits a strong lateral gradient in salinity from almost freshwater conditions in its northern and eastern interior regions (<3 psu [= practical salinity units; Millero et al., 2008]) to intermittently normal marine conditions around the Danish Straits (~30–35 psu)

* Corresponding author.
*E-mail address:* mremirez@gmu.edu (M.N. Remírez).

https://doi.org/10.1016/j.palaeo.2024.112216
Received 18 September 2023; Received in revised form 20 February 2024; Accepted 16 April 2024
Available online 20 April 2024

(Voipio, 1981). In contrast, the Persian/Arabian Gulf, located in an arid climate belt, exhibits surface salinities of 38–40 psu, with salinities up to ~50 psu in nearshore areas and > 100 psu in tidal-flat porewaters (Reynolds, 1993; Hassanzadeh et al., 2011). On the other hand, the Gulf of Carpentaria in northern Australia, which is better connected to the global ocean than either the Baltic Sea or Persian/Arabian Gulf, exhibits almost uniformly normal marine salinities, i.e., ~35 psu (Somers and Long, 1994). However, salinity conditions in modern epeiric seas have changed frequently in the past owing to sea-level fluctuations, e.g., both the Baltic Sea and Gulf of Carpentaria experienced a transition from a freshwater lake environment as a result of rising sea level at ca. 11–9 ka (Berglund et al., 2005; Chivas et al., 2001). Thus, the evidence from modern epeiric seas suggests that complex spatio-temporal patterns of salinity variation may have developed in ancient epeiric seas (Weckström et al., 2017; Reeves et al., 2008).

The Neuquén Basin of Argentina-Chile contains a near-continuous record of marine and continental sedimentation from the Late Triassic to the early Paleogene (Howell et al., 2005). The basin experienced unambiguous marine transgressions from the Panthalassic Ocean during the Pliensbachian-Bathonian, Tithonian-Berriasian, and Valanginian-Barremian, resulting in accumulation of richly fossiliferous marine deposits (Gasparini and Fernández, 2005; Riccardi et al., 1999; Aguirre-Urreta et al., 2011). The Arroyo Malo Formation (AMF), which spans the Triassic-Jurassic boundary, contains a sparse marine fauna and has long been considered to record the earliest marine transgression in the Neuquén Basin on that basis (Riccardi et al., 2004), implying a connection with the Panthalassic Ocean (Bechis et al., 2020) and representing the only putatively marine record among numerous continental basins of Late Triassic age in western South America (Franzese et al., 2003). In this contribution, through the use of elemental proxies, we re-evaluate the salinity conditions of the AMF, demonstrating its accumulation under freshwater to low-brackish conditions, and their implications for the timing of opening of the Neuquén Basin. This study is an example of the importance of assessing salinity as a proxy for unravelling the connection of ancient epeiric seas with the open ocean, as well as to improve our understanding of the initial phases of marine basins.

## 2. Geologic setting

### 2.1. The Neuquén Basin

The Neuquén Basin, located in west-central Argentina and adjacent Chile (Fig. 1A), represents a thick succession of marine and continental deposits of Triassic to Cenozoic age (Howell et al., 2005). During the Late Triassic to Early Jurassic, the southwestern margin of Gondwana was characterized by an extensional regime, resulting in formation of multiple rift basins (depocenters) that accumulated thick volcaniclastic

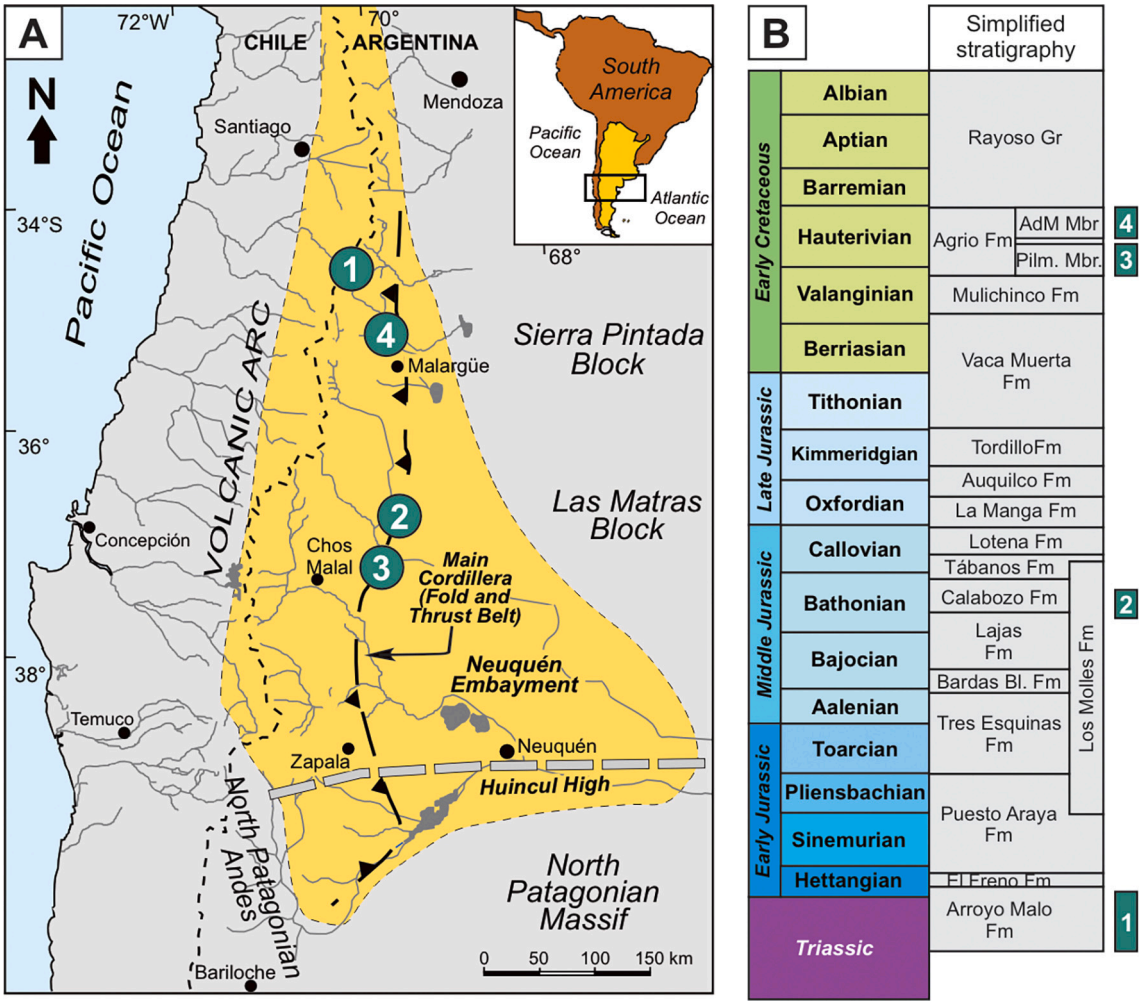


**Fig. 1. (A)** Location of the Neuquén Basin and the study area (modified from Schwarz et al., 2022). 1) Arroyo Malo Formation (Atuel Depocenter), 2) Los Molles Formation (note: the study samples from this unit are Bathonian in age), 3) Pilmatué Member, Agrio Formation, 4) Agua de la Mula Member, Agrio Formation. **(B)** Stratigraphy of the of the Neuquén Basin. Green bars at right show the study intervals. AdM Mbr = Agua de la Mula Member; Pilm. Mbr = Pilmatué Member. (For interpretation of the references to colour in this figure legend, the reader is referred to the web version of this article.)

and epiclastic continental deposits (Franzese et al., 2003). In the northern Neuquén Basin (Mendoza Province), the Malargüe-Llantenes Depocenter accumulated fluvio-lacustrine sediments of the Tronquimal Group (Artabe et al., 1998), while the Atuel Depocenter hosted the putatively marine AMF (Spalletti, 1997; Morel et al., 2003; Riccardi, 2019). Subsequently, during the Early Jurassic-Early Cretaceous, the Neuquén Basin developed into a back-arc basin accumulating intercalated marine and continental deposits (Vergani et al., 1995; Howell et al., 2005). This basin was subject to episodic marine transgressions, the earliest of which is thought to have been recorded by the AMF (Riccardi et al., 1997). This formation consists of ~300 m of shale interbedded with thin beds of siltstone and sandstone, organized into coarsening- and thickening-upward cycles that were interpreted as deposits of a marginal-marine basin proximal to fluvial-dominated slope-type fan deltas (Lanés, 2005).

### 2.2. Ages of study units

Within the Arroyo Malo Formation, the position of the Triassic-Jurassic boundary has long been based on bivalve, brachiopod, and ammonoid faunas (Fig. 2; Riccardi et al., 1991; Riccardi et al., 2004), although it was more recently constrained by the last appearance of Rhaetian-age bivalves (*Septocardia peruviana*, *Paleocardita peruviana*) and brachiopods (*Zugmayerella koerneri*), and by the first appearance of Hettangian bivalves (*Palmoxytoma* cf. *cygnipes, Eopecten* cf. *velatus,* and *Camptonectes?* cf. *subulatus*) and brachiopods (*Furcirhynchia* cf. *trechamanni* and *Lingula* cf. *metensis*) (Riccardi et al., 1991; Damborenea and Manceñido, 2012; Damborenea et al., 2017). A recent study identified the Rhaetian taxa *Rabdoceras suessi* at 73 m and *Aulacoceras* cf. *carlottense* at 66 and 73 m, followed by the Hettangian taxa *Psiloceras* cf. *primocostatum* at 188 m and *P.* cf. *polymorphum* at 191 and 197 m

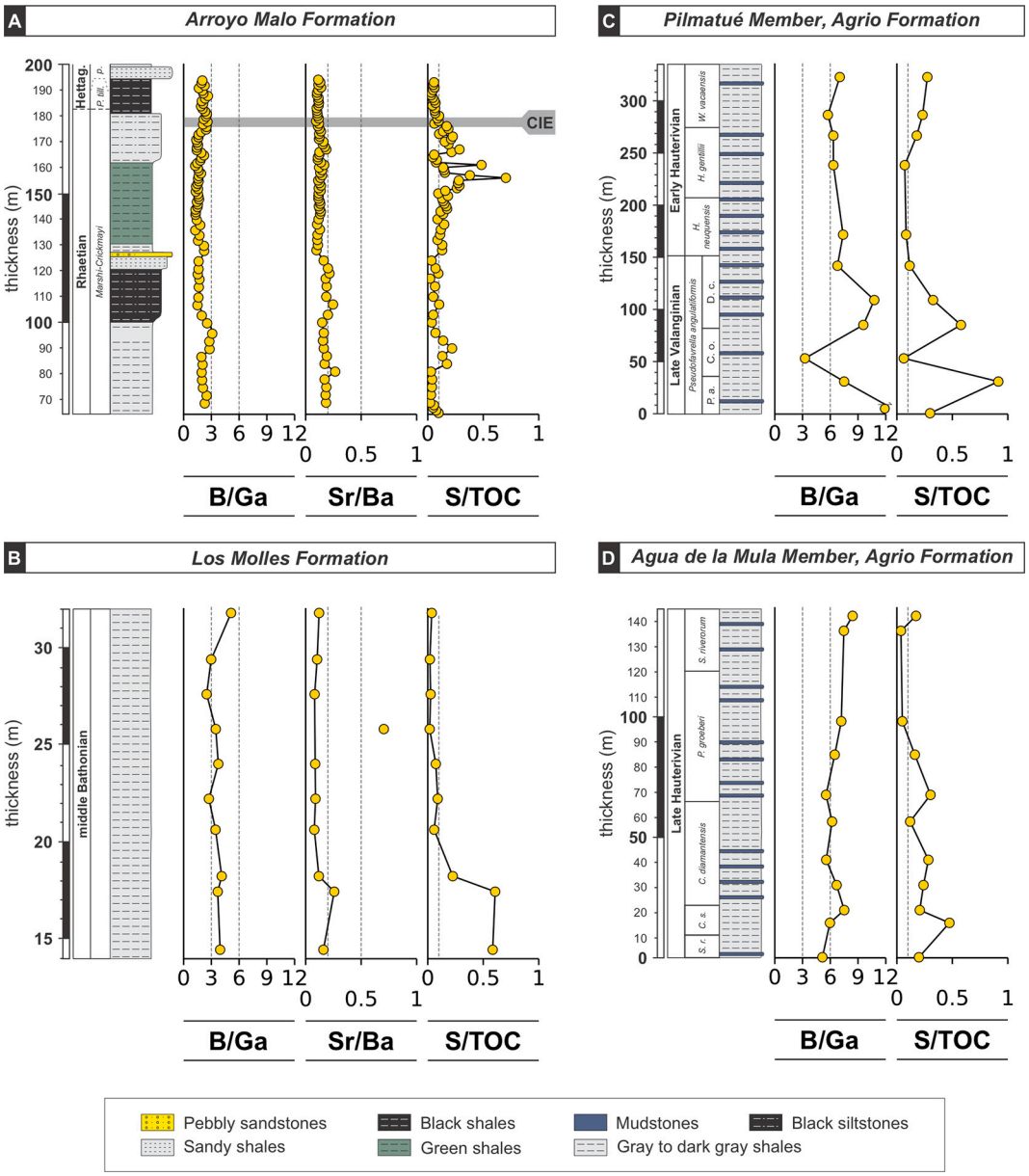


**Fig. 2.** **(A)** Paleosalinity proxies (B/Ga, Sr/Ba, and S/TOC) for the TJT Arroyo Malo Formation show a consistent trend toward freshwater conditions with occasional excursions to low-brackish conditions (biostratigraphy from Damborenea et al., 2017, and Ruhl et al., 2020). *P. til.* = *Psiloceras tilmani, p.* = *Psiloceras primocostatum*). CIE = Triassic-Jurassic boundary carbon isotope excursion. Paleosalinity proxies for **(B)** Los Molles Formation, **(C)** Pilmatué Member (biostratigraphy from Aguirre-Urreta et al., 2019), *P. a.* = *Pseudofavrella angulatiformis, C. o.* = *Chacantuceras ornatum, D. c.* = *Decliveites crassicostratum*), and **(D)** Agua de la Mula Member (biostratigraphy from Aguirre-Urreta et al., 2019), *S. r.* = *Spitidiscus ricardii, C. s.* = *Crioceratites schlangintweiti*) suggest an increase in salinity that was probably related to a better connection with the Panthalassic Ocean. Sr/Ba is not displayed in panels C and D due to the large carbonate influence on Sr content.

(Riccardi, 2019). The characteristic uppermost Triassic $\delta^{13}C_{org}$ excursion, which is located between 175 and 179 m in our measured section (Fig. 2), helped in refining placement of the TJB at ~183 m (Ruhl et al., 2020).

The Los Molles Formation is above the Bardas Blancas Formation and below the Lajas Formation in the study area (Fig. 1). It is barren of macrofossils, but ammonites have been reported from the upper part of the Bardas Blancas Formation (*Morphoceras* sp., *Phylloceras* sp., and *Lytoceras* cf. *eudesianum*) and the lower part of the Lajas Formation (*Iniskinites crassus*, *Stehnocephalites gerthi*, and *Lilloettia* cf. *steinmanni*), consistent with a middle Bathonian age (Spalletti et al., 2012).

The Pilmatué Member of the Agrio Formation is late Valanginian to early Hauterivian in age in the study area, as determined from astrochronology, U—Pb ages, and ammonite and calcareous nannofossil biostratigraphy (Aguirre-Urreta et al., 2019). The *Pseudofavrella angulatiformis* ammonite Zone is recognized by the presence of abundant flattened impressions of *Viluceras permolestus* near the base of the unit, whereas its upper part is characterized by the presence of abundant ammonites defining the *Weavericeras vacaensis* ammonite Zone (Aguirre-Urreta et al., 2019). The middle part of the unit yielded a U—Pb CA-ID-TIMS age of 139.39 ± 0.16 Ma (Aguirre-Urreta et al., 2019).

The Agua de la Mula Member of the Agrio Formation lacks biostratigraphic data in the study area. However, the age of this unit has been studied in detail at another location (ca. 200 km southward) through a combination of astrochronology and ammonite and calcareous nannofossil biostratigraphy, and this age framework has been extrapolated to the present study locale, since the lithology and thickness of this unit is nearly the same in both areas (Remírez et al., 2022a). Thus, this unit is assigned to the late Hauterivian. The lowermost ammonite biozone is the *Spitidiscus ricardi* Zone, as indicated by the presence of small specimens and flattened impressions of *Spitidiscus* spp. near the base of the unit, and the uppermost biozone is the *Sabaudiella riverorum* ammonite Subzone, as indicated by the presence of its index species (Aguirre-Urreta et al., 2019; Marin et al., 2023).

## 3. Methods

### 3.1. Sample collection

The present study section (Arroyo Alumbre) at Estancia El Sosneado (34°49′28" S, 69°53′01" W, Fig. 1) is located in the Atuel Depocenter of the northern Neuquén Basin. It has been extensively studied with regard to its paleobiological (Riccardi and Iglesia Llanos, 1999; Riccardi et al., 1997, 2004; Manceñido and Damborene, 2005; Damborenea and Manceñido, 2012; Damborenea et al., 2017; Echevarría et al., 2017) and sedimentological features (Lanés, 2005; Lanés et al., 2008). For the AMF, we generated a detailed lithostratigraphic log and collected 130 samples at one-meter intervals in the Arroyo Alumbre section (from 65 m to 193 m above the section base; Fig. 2). We also collected 10, 11, and 11 samples from three auxiliary units: (1) the Lower-Middle Jurassic (Pliensbachian-Callovian) Los Molles Formation (LMF) at Agua del Ñaco in the eastern Sierra de Reyes (36°30′ S, 69°30′ W); (2) the Lower Cretaceous (Valanginian-Hauterivian) Pilmatué Member (PM) of the Agrio Formation at El Portón (37°09′S, 69°41′W); and (3) the Lower Cretaceous (Hauterivian) Agua de la Mula Member (AM) of the Agrio Formation at Arroyo Cienaguitas (35°12′S, 69°46′W) (Fig. 1A). C and S concentrations were analyzed for all samples (see Supplemental Material), and minor and trace elements were analyzed for 80 AMF samples and 32 auxiliary samples.

### 3.2. C—S analysis

Non-acid volatile sulfur (NAVS) and total organic carbon (TOC) were determined using an Eltra C/S 2000 Analyzer at the University of Cincinnati. Sample preparation entailed weighing out ~100 mg of powder, decarbonation with dilute (10%) hydrochloric acid over a hot plate (~75 °C) for 6 h, filtering and rinsing repeatedly with deionized water, and then drying in an oven (~75 °C) overnight. Samples were calibrated with external (USGS SDO-1, C = 9.68%, S = 5.35%) and internal (DBS-1, C = 3.50%, S = 1.97%) laboratory standards, and analytical precision (2σ) based on replicate analyses was ±2% and ±5% of measured values for C and S measurements, respectively.

### 3.3. Elemental geochemistry

Elemental concentrations (B, Ga, Sr, Ba, Mo, U, Al, and P) were measured using an Agilent 7500a inductively coupled plasma mass spectrometer (ICP-MS) at the State Key Laboratory of Geological Processes and Mineral Resources (GPMR) of the China University of Geosciences-Wuhan. About 50 mg of sample powder were weighed into a Teflon bomb, and 1 mL $HNO_3$ and 1 mL HF were added before heating for ~48 h at 190 °C in the sealed bomb. After cooling, the contents of the bomb were evaporated at 115 °C to incipient dryness, and 1 mL $HNO_3$ and 1 mL 1-ppm indium (In) laboratory standard were added. The bomb was then resealed and heated to 190 °C for another 12 h. The final solution was transferred to a polyethylene bottle and diluted in 2% $HNO_3$ to about 100 mL for ICP-MS analysis. Results were calibrated using the international standards AGV-2, BHVO-2, BCR-2, RGM-1, and GSR-1 with an average analytical uncertainty better than 2% (RSD). Mo and U enrichment factors were calculated following the methodology described in Tribovillard et al. (2006), where enrichment factor (EF) is $EF_X = ([X]_{sample}/[Al]_{sample}) / ([X]_{standard}/[Al]_{standard})$ and the reference standard is average shale (Mo = 1.3 ppm, U = 3 ppm, Al = 88,900 ppm, Wedepohl, 1991). Also, normalization of these metals with Th was also performed. These elements (as well as other transition metals) are generally soluble under oxic conditions yet become particle-reactive and are removed from solution in the presence of a variety of reductants, thus enriching sediments in Mo, U, V, and Re (and others) under reducing conditions. Molybdenum enrichment requires euxinia, although U enrichment requires only general anoxia (Tribovillard et al., 2006; Algeo and Liu, 2020; Bennett and Canfield, 2020). The $C_{org}$/P ratio is a molar ratio that relies on the different rates at which organic carbon and phosphorus are remineralized under different redox conditions (Algeo and Ingall, 2007). If conditions are reducing, the preservation of organic carbon is improved, but reactive phosphorus tends to be released from sediments back to the water column, causing sediment $C_{org}$/P ratios to increase compared to the ratio of marine phytoplankton biomass, which is approximately 106:1 (known as the Redfield ratio; Redfield, 1963).

## 4. Results and interpretations

### 4.1. Paleosalinity proxies

In the AMF, elemental paleosalinity proxies exhibit almost uniformly low values. B/Ga averages 2.0 (range 1.6–2.4), with nearly all samples below the freshwater-brackish threshold of 3 (Wei and Algeo, 2020) (Figs. 2 and 3). Sr/Ba averages 0.14 (range 0.11–0.17), with most samples below the freshwater-brackish threshold of 0.2 (Fig. 2A). The highest values (0.20–0.26) are associated with high B/Ga (Fig. 2A). Sr/Ba is not visibly affected by carbonate-hosted Sr (Fig. 4). S/TOC averages 0.11 (range 0.04–0.18), with samples approximately bracketing the freshwater-brackish threshold of 0.1 (Fig. 2A; Wei and Algeo, 2020). Higher S/TOC values are recorded between 80 and 100 m (average 0.15), coincident with the highest B/Ga values (Fig. 2A), and between 125 and 175 m, where a few isolated samples exceeded typical freshwater salinity values ($n$ = 2; Fig. 2A). These salinity proxy results strongly indicate that the AMF was a dominantly freshwater unit (<1 psu), possibly subject to infrequent brackish episodes.

In contrast to the largely freshwater conditions of the AMF (Triassic-Jurassic boundary), all younger shale units in the Neuquén Basin (i.e., of Middle Jurassic to Early Cretaceous age) have much higher means

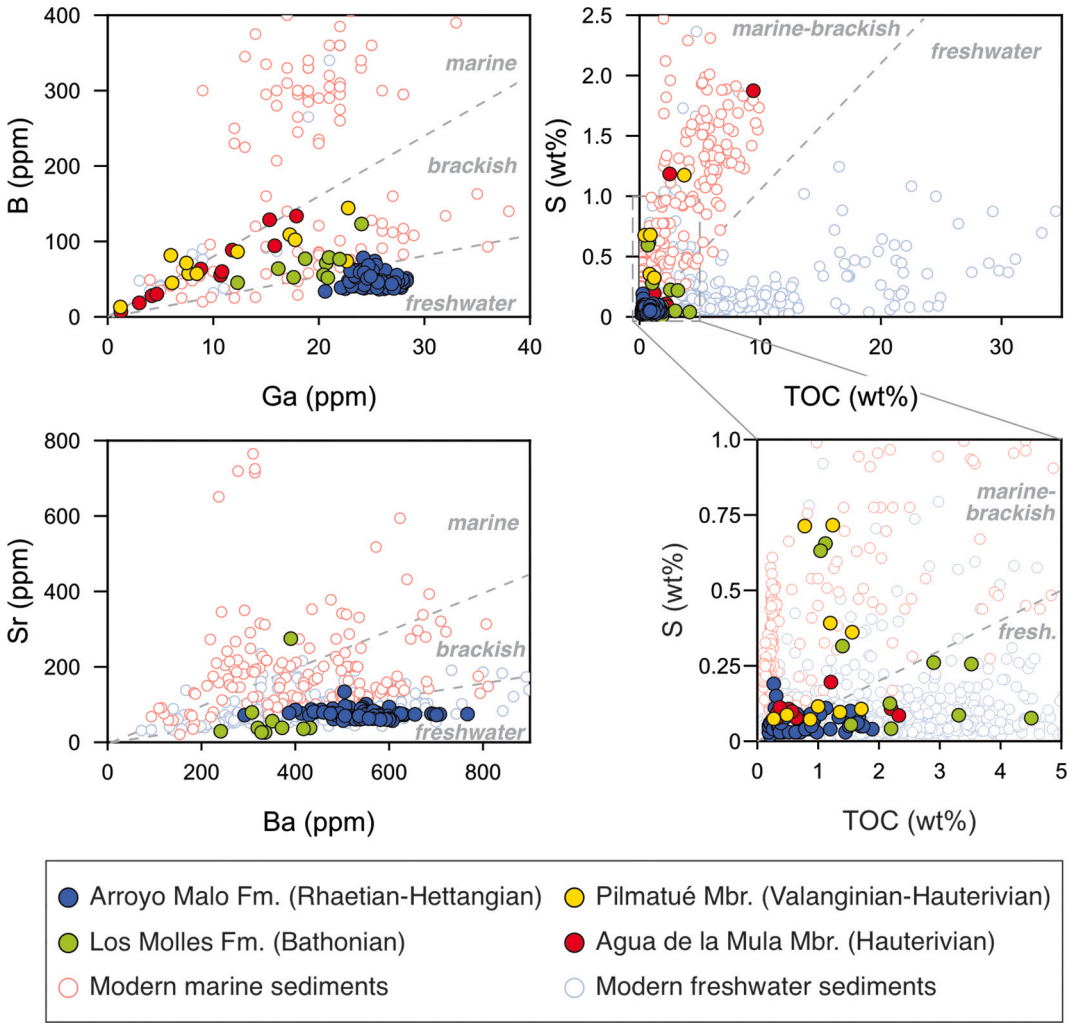


**Fig. 3.** Boron-vs-gallium, strontium-vs-barium, and sulfur-vs-TOC relationships in the study sections, compared with data for modern freshwater and marine sediments (from Wei and Algeo, 2020).

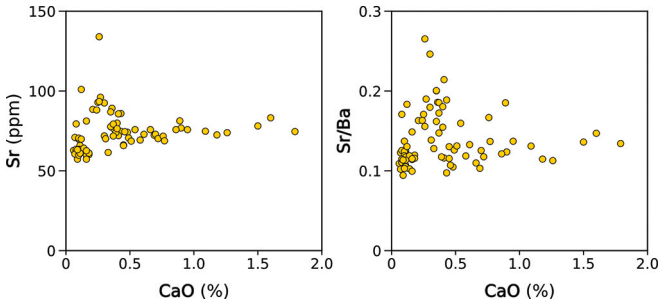


**Fig. 4.** Sr and Sr/Ba vs. CaO crossplots for the AMF indicating no relationship of Sr or Sr/Ba with carbonate content, and thus the reliability of Sr/Ba as a salinity proxy (cf. Wei and Algeo, 2020).

(ranges) of salinity proxy values: (1) the Lower-Middle Jurassic (Pliensbachian-Callovian; note: samples are from the Bathonian part of formation) Los Molles Formation (LMF) yields B/Ga of 3.50 (2.5–5.1), Sr/Ba of 0.12 (0.08–0.26; note: a single outlier at 0.7 is likely due to carbonate-hosted Sr), and S/TOC of 0.17 (0.02–0.60; Fig. 2A), implying low-brackish conditions (~1–10 psu); (2) the Lower Cretaceous (Valanginian-Hauterivian) Pilmatué Member (PM) of the Agrio Formation yields B/Ga of 7.7 (3.3–13.6), Sr/Ba is indeterminate (too much carbonate-hosted Sr is present; Moore et al., 2020; Remírez et al., 2022b), and S/TOC of 0.28 (0.06–0.91; Fig. 2B), implying fully marine conditions (~30–40 psu); and (3) the Lower Cretaceous (Hauterivian) Agua de la Mula Member (AM) of the Agrio Formation yields B/Ga of 6.5 (5.1–8.4), Sr/Ba is again indeterminate (due to carbonate content: Moore et al., 2020; Remírez et al., 2022a), and S/TOC of 0.20 (range 0.04–0.47; Fig. 2C), also implying dominantly marine conditions although possibly punctuated by intermittent high-brackish episodes (~10–30 psu).

### 4.2. Redox proxies

In the Arroyo Malo Fm., most samples yield enrichment factors of molybdenum ($Mo_{EF}$) below 2.0, indicating no significant enrichment relative to average shale (Fig. 5A). Only a handful of samples yield higher $Mo_{EF}$ (~2–5), including samples at 87 and 121 m and in the interval from 157 m to 185 m (13 out of 37 samples). Enrichment factors of uranium ($U_{EF}$) are all between 0.5 and 1.5 (Fig. 5A), indicating no significant enrichment. $C_{org}$/P ratios are mostly <50, indicating well-oxidized conditions (Fig. 5A). The highest $C_{org}$/P ratios (~100–150) mostly correspond to intervals of high TOC (72, 81, 100 and 124 m), suggesting slightly reducing conditions.

Mo/Th and U/Th show very low values in the Arroyo Malo Fm. (median 0.07 and 0.25, respectively), which also confirms the lack of enrichment in redox-sensitive elements. In the Los Molles Formation, both Mo/Th and U/Th show very low values (median = 0.39 and 0.38,

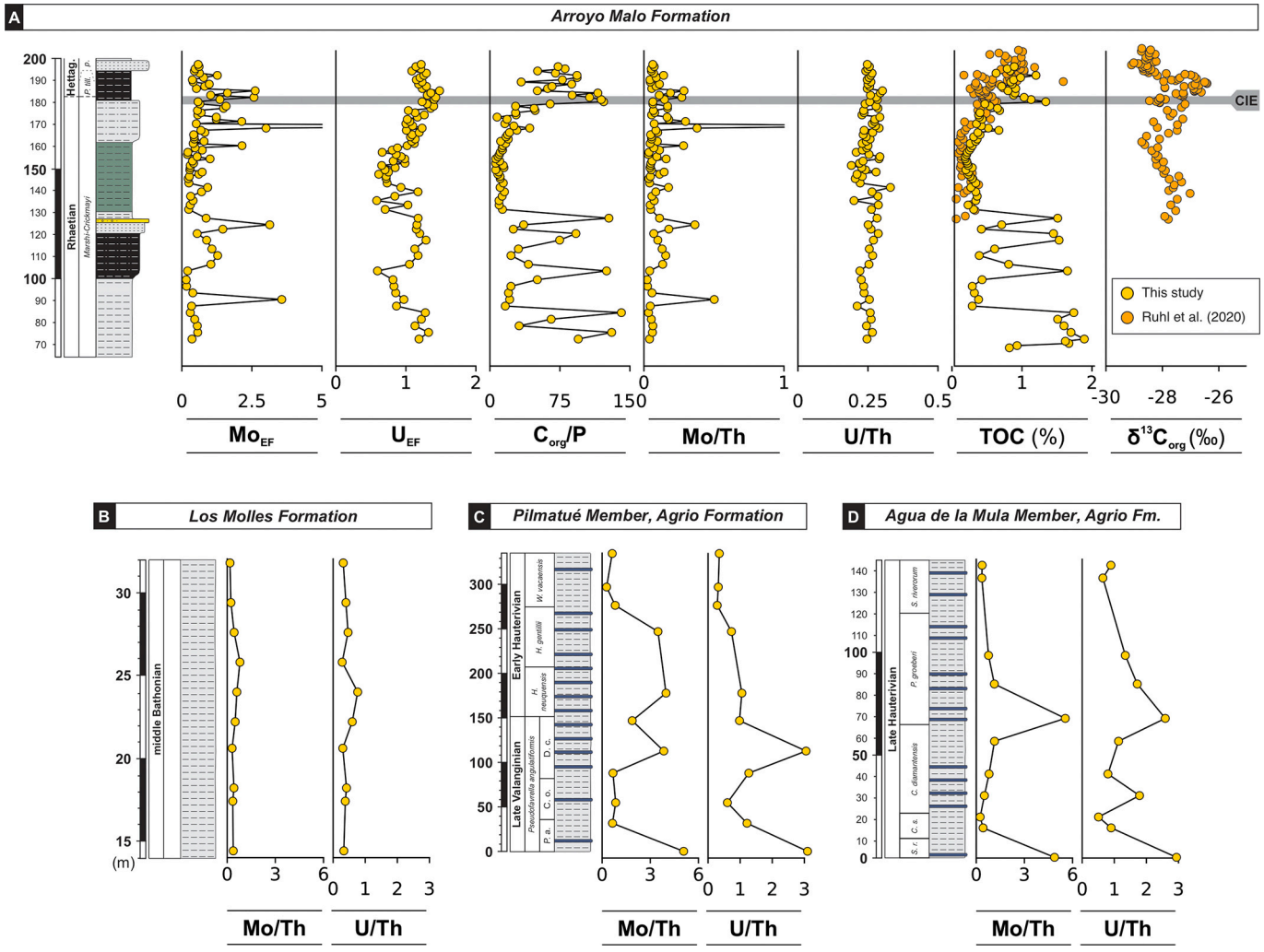


**Fig. 5. (A)** Mo and U enrichment factors, $C_{org}/P$, Mo/Th, U/Th, TOC, and $\delta^{13}C_{org}$ (Ruhl et al., 2020) for the Arroyo Malo Formation reveal consistently well-oxygenated watermasses during most of the Rhaetian. Slight increases in $C_{org}/P$ (to just above the Redfield ratio) and TOC content coincident with the Late Triassic carbon isotope excursion is the only interval in which suboxic conditions existed. **(B)** Mo/Th and U/Th for the Los Molles Formation suggest a well-oxygenated water column during sediment deposition. **(C)** Mo/Th and U/Th for the Pilmatué Member show variations in water-column oxygenation, and **(D)** Mo/Th and U/Th for the Agua de la Mula Member suggest episodic low-oxygen conditions. For abbreviations and references, see Fig. 2.

respectively), suggesting well-oxygenated conditions (Fig. 5B). The Pilmatué and Agua de la Mula members show higher medians for Mo/Th and U/Th (0.84 and 0.98, and 0.76 and 1.13, respectively) influenced by enrichment in some intervals that likely represent episodic development of suboxic to anoxic conditions in a generally well-oxygenated setting (Fig. 5C-D).

## 5. Discussion

### 5.1. Potential diagenetic effects on shale salinity proxies

Since our paleosalinity interpretations rely on geochemical proxies, we will briefly consider whether preserved signals might have been altered by secondary processes. The thresholds of B/Ga salinity facies have an accuracy around 88% in modern muddy sediments (Wei and Algeo, 2020), and the B/Ga proxy has been demonstrated to be highly sensitive to subtle salinity variations (Remírez and Algeo, 2020). Boron is adsorbed by clay minerals (into interlayer sites or displacement of $H_2O$ and $OH^-$ from surface $\alpha$-$Al_2O_3$ sites) or incorporated into tetrahedral sites of the clay mineral structure (Keren and Mezuman, 1981; Mackin, 1987; Williams et al., 2001; Williams and Hervig, 2002; Muttik et al., 2011). Furthermore, it is also common to find small amounts of boron in other phases such as Fe and Mn-oxyhydroxides (Donahoe and Liu, 1998). The most important host of boron in sediments is generally illite and mixed-layered illite/smectite (up to ~80% of total B), whereas kaolinite and chlorite generally contain only minor amounts (Perry, 1972). During burial, boron in interlayer sites can undergo adsorption-desorption processes (You et al., 1996), resulting in its possible loss at high temperatures and pressures (Williams et al., 2001, 2007; Williams and Hervig, 2005; Deyhle and Kopf, 2005; Środoń and Paszkowski, 2011). However, primary boron signals may be preserved during the process of illitization, in which boron is transferred from interlayer sites in smectite to structural sites in illite, a process that can quantitatively retain boron under closed porewater conditions (Perry, 1972; Spivack and Edmond, 1987; Williams et al., 2001). In general, boron is not easily leached from structural sites, even under acidic conditions (Villumsen and Nielsen, 1976).

Gallium is commonly present in detrital clay mineral phases, and its chemistry is controlled by aluminum owing to substitution of $Ga^{3+}$ for $Al^{3+}$ (Wang et al., 2011; Breiter et al., 2013). Although less reactive than boron, aqueous gallium can be adsorbed onto clay minerals, but low gallium concentrations in most watermasses preclude significant secondary enrichment (Shiller and Frilot, 1996; Foley et al., 2017). In the sediment, gallium tends to be immobile during diagenesis (Panahi et al.,

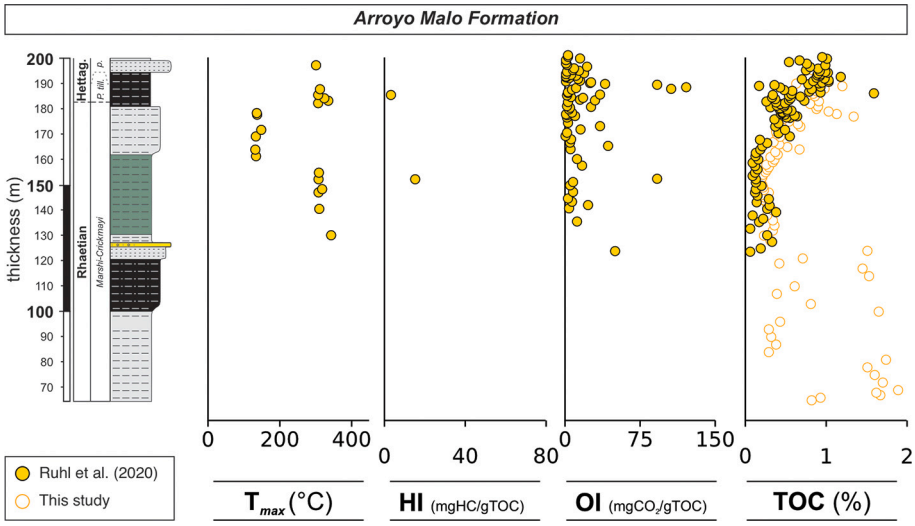


**Fig. 6.** $T_{max}$, Hydrogen index (HI), oxygen index (OI), and total organic carbon (TOC) for the study section (data from Ruhl et al., 2020).

2000), especially under alkaline porewater conditions as are common in marine systems (Rytuba et al., 2003). In general, gallium concentrations are much less variable in shales than boron concentrations, suggesting that gallium provides a stable denominator against which to evaluate salinity changes recorded by adsorbed boron (Remírez and Algeo, 2020). This pattern is observed in the Arroyo Malo Fm. (Ga range = 20.6–28.3 ppm; B range = 30.8–78.2 ppm; Supplemental Material).

The S/TOC proxy is highly effective at distinguishing freshwater from more-saline facies, with an accuracy of ~91% in modern muddy sediments, but it is not robust in distinguishing brackish from marine facies (Wei and Algeo, 2020). During burial diagenesis, both S and TOC content can be affected, especially due to increasing temperatures that lead to thermochemical sulfate reduction, which reduces sedimentary sulfur concentrations (Machel, 2001; Watanabe et al., 2009). Similarly, burial diagenesis can degrade the organic fraction of the sediment, but its effects are related to the type of organic matter present (Tyson, 2012).

Sr/Ba can discriminate freshwater, brackish, and marine salinity facies, but its accuracy (~66%) is lower than that of B/Ga in modern muddy sediments (Wei and Algeo, 2020). During burial diagenesis, strontium can be released from the host phase by degradation of organic matter, dehydration and/or illitization of clay minerals, as well as by dissolution and/or albitization of plagioclase and K-feldspar (Sullivan et al., 1990; Feldman et al., 1993; Salminen et al., 2005; Yang et al., 2004a, 2004b, 2006). Nevertheless, Ca-bearing minerals such as carbonates and authigenic albite can incorporate the leached Sr into diagenetic phases, limiting its diffusion out of the sediment (Feldman et al., 1993). Similarly, barium can be remobilized during burial diagenesis, especially from reduction of barite (common in organic-rich sediments) in anoxic bottom waters or porewaters during early diagenesis (Dymond et al., 1992; Salminen et al., 2005; Holland and Turekian, 2010). However, diagenetic transformation of clay and silicate minerals can release barium during the late diagenetic stage (Holland and Turekian, 2010). A common problem in use of Sr/Ba ratios as a salinity proxy in shales is the presence of strontium sourced from carbonate phases (Wei and Algeo, 2020). The present study section exhibits values of CaO below 2 wt.% (average shale ~3 wt.%) as well as a lack of a linear covariation between Sr and CaO (Fig. 4), consistent with its Sr content being hosted dominantly by the clay fraction and not sourced from carbonate components in the sediment.

The possibility of thermal alteration of salinity proxy signals should be considered, although the thermal history of the study section is not well constrained. The 250-m-thick succession of the Triassic-Jurassic Arroyo Malo Formation in the Arroyo Alumbre section is assumed to have experienced a relatively uniform burial and thermal alteration history. The tectonic history of the Atuel depocenter started with a rifting phase during the Late Triassic that developed several small depocenters along the southwestern margin of Gondwana (Vergani et al., 1995; Howell et al., 2005). Following the Early Jurassic, active subduction led to the development of the Andean magmatic arc along the western margin of this supercontinent (Mpodozis and Ramos, 1990), behind which formed thermal subsidence-controlled and connected back-arc basins (Howell et al., 2005). During the Late Cretaceous, the Andean Orogeny began (Zapata and Folguera, 2005), with multiple stages extending to the Miocene and recent (see Bechis et al., 2020, for a recent review). Various deformation pulses associated with thermal maturation of the sedimentary succession are thought to have been responsible for thermal degradation of organic matter and alteration of mineralogical assemblages (Percival et al., 2017; Ruhl et al., 2020). To date, however, no studies have carried out a systematic analysis of the burial history of the study area.

The organic fractions of the study units were characterized in greater detail by Ruhl et al. (2020). Rock-Eval analysis yielded TOC values ranging from 0.06 and 1.59wt.% (average = 0.56wt.%, $16^{th}$ percentile = 0.18wt.%, $84^{th}$ percentile = 0.92wt.%), which are similar to our results (range 0.15 to 1.89wt.%, average = 0.66wt.%, $16^{th}$ percentile = 0.26wt.%, $84^{th}$ percentile = 1.15wt.%). Oxygen index (OI) values range from 0.5 to 206 mg $CO_2$/g TOC (average = 24.6, $16^{th}$ percentile = 2.0, $84^{th}$ percentile = 44.7), and $T_{max}$ values from 128 to 577 °C (average = 295 °C, $16^{th}$ percentile = 131 °C, $84^{th}$ percentile = 449 °C; Fig. 6). Samples from below 200 m in the Ruhl et al. (2020) study (their Fig. 2) are equivalent to the present study section (Fig. 6). Sources rocks are considered overmature if $T_{max}$ values exceed 450, 460, and 470 °C for kerogen types I, II and III, respectively (Nali et al., 2000). Apart from four samples (out of 22) located between 164.4 and 180.9 m (~600 °C), all samples of the Arroyo Malo Fm. yielded $T_{max}$ values below 400 °C, with many values around 330 °C (Ruhl et al., 2020) (Fig. 6). Sample-to-sample variations in $T_{max}$ values were probably influenced by factors such as oxidation and/or reworking of the original organic matter (Yang and Horsfield, 2020), because the samples with higher $T_{max}$ values come from a fine-grained sandstone facies with slump folds and plant remains (Lanés, 2002; Lanés et al., 2008). However, low values of OI as well as hydrogen index (only analyzed in two samples, both below 15 mg $CO_2$/g TOC) possibly indicate intense degradation of the original organic matter. Significantly, however, any changes in clay-mineral assemblages and/or the organic fraction due to thermal burial effects should have been relatively uniform throughout the entire section.

### 5.2. The salinity evolution of the Neuquén Basin

The AMF has never been deeply buried, and the consistency of the paleosalinity interpretations yielded by the three elemental proxies argues strongly for preservation of a primary salinity signature. The majority of samples from this formation exhibit freshwater values for all proxies (79 of 80 of B/Ga; 75 of 80 of Sr/Ba; 70 of 130 of S/TOC), and the remainder yield mixed freshwater-brackish values, based on the salinity facies thresholds of Wei and Algeo (2020). On this basis, we infer a dominantly freshwater environment that may have shifted occasionally to low-brackish conditions. Such conditions are consistent with the more proximal (i.e., landward) regions of a large estuary such as the Chesapeake Bay (Pritchard, 1952). Our findings disprove a previous model for the AMF that inferred a fluvio-dominated slope-type fan delta within a basin of fully marine salinity (Lanés, 2005; Riccardi et al., 2004), suggesting instead that the delta was likely a dominantly freshwater environment.

The Mesozoic Neuquén Basin was a relatively small, shallow epicontinental sea influenced by both freshwater influx and evaporation, potentially causing salinity to vary in both space and time (Schwarz et al., 2022). Earlier interpretations of marine conditions for the Triassic-Jurassic boundary deposits of the Neuquén Basin were based largely on the presence of small numbers of putatively marine fossils (Fig. 7). Reported sedimentological features such as high mudstone abundance, the presence of low-density turbidite and cohesive debris flows, and the absence of tidal and wave structures (Lanés, 2005) are not diagnostic of depositional environment. The relatively consistent orientation of paleocurrent structures indicates basin deepening toward the W-SW in the middle part of the section, rotating toward the W-NW in its upper part, but this pattern could have been produced either in a slope fan-delta (Lanés, 2005; Bechis et al., 2020) or an estuarine system (Hanebuth et al., 2012). In any case, low salinities near freshwater conditions could be possible (Fig. 8).

For the younger stratigraphic units analyzed in this study, the elemental salinity proxies suggest a progressive evolution from low-brackish conditions in the Middle Jurassic LMF to high-brackish or fully marine conditions in the Lower Cretaceous PM and AM (Fig. 8). The LMF was deposited during a major transgression of the Neuquén Basin (Vergani et al., 1995), where the influence of fluvial freshwater discharge was inferred from palynological studies (Martínez et al., 2008; Olivera et al., 2020). However, our results suggest low bottom-water salinity values for this unit, whereas a previous study inferred salinity reduction only in the surface layer with normal-marine conditions in the deeper watermass (Olivera et al., 2020). Open-ocean circulation is contradictory with low-brackish values, and freshwater discharge was probably more important than previously assumed, at least for the northern Neuquén Basin. The LMF has been regarded as fully marine based largely on fossil content (Riccardi et al., 2011), but it seems likely that freshwater discharge into a relatively small basin (Privat et al., 2021) reduced the salinity of the entire watermass (Fig. 8). Moreover, the LMF study section is barren of macrofossils (Spalletti et al., 2012). On the other hand, our salinity interpretations for the PM and AM are consistent with those of previous studies, which have inferred fully marine conditions on the basis of fossil content (e.g., Lazo et al., 2005) and oyster-shell oxygen isotopes (Lazo et al., 2008). The salinity proxy data of the present study document progressively greater marine

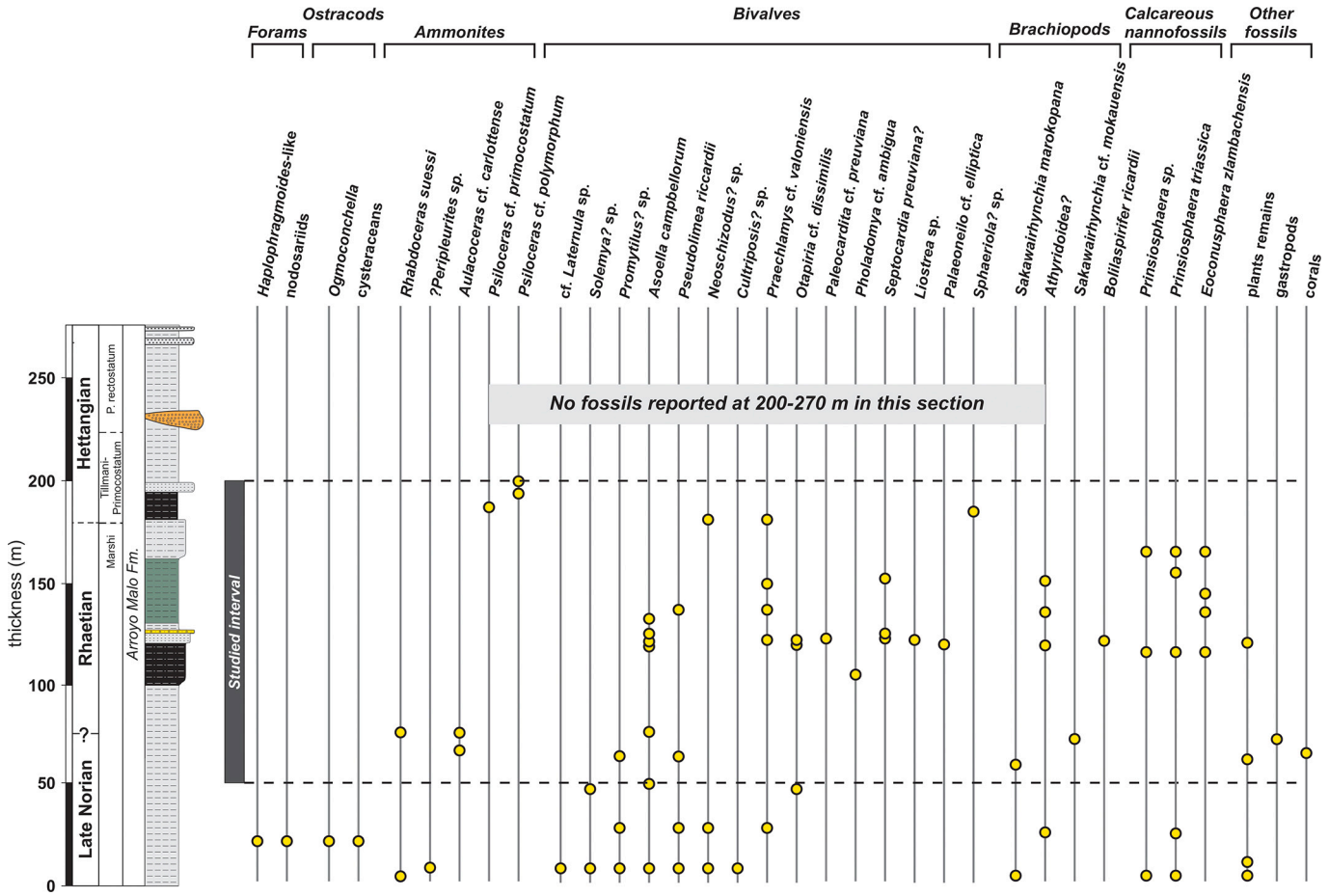


**Fig. 7.** Fossil distribution in the Arroyo Malo Formation at the Arroyo Alumbre section in southern Mendoza Province (northern Neuquén Basin). The fossils record is sparse and highly fragmented, which suggests strong reworking and transport before final deposition. Fossil data are from Riccardi et al. (2004), Damborenea et al. (2017), Riccardi (2019), and Pérez Panera et al. (2023).

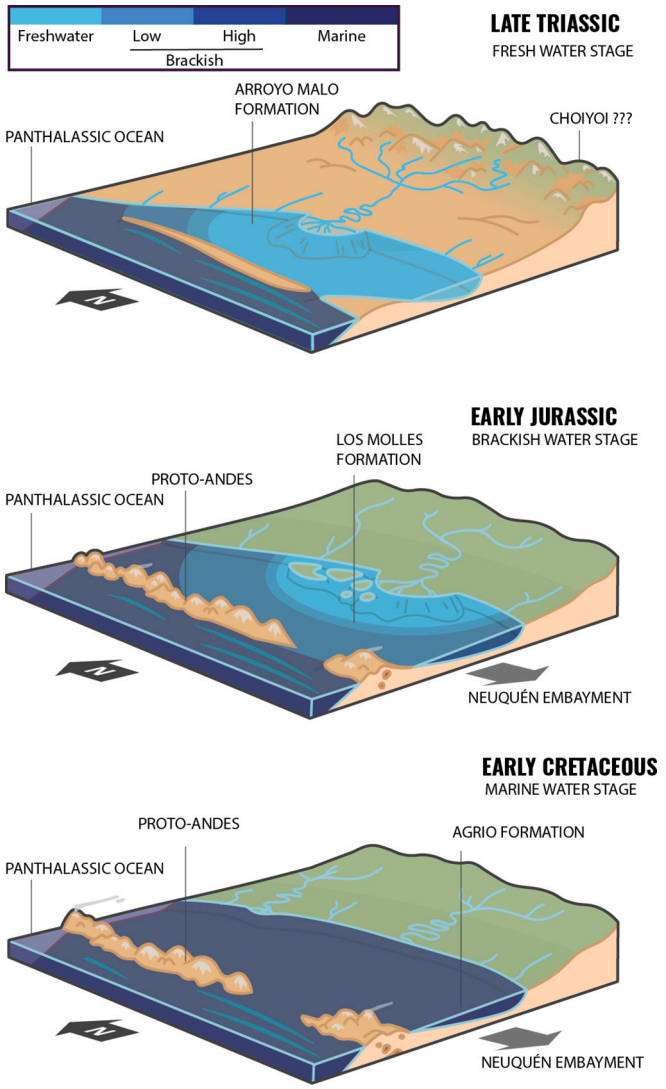


**Fig. 8.** Paleogeographic reconstruction of the Neuquén Basin from the Late Triassic to Early Cretaceous. The basin opened progressively to the Panthalassic Ocean during this interval, producing fully marine conditions by the Cretaceous (reconstructions based on Howell et al. (2005), Olivera et al. (2020), Lazo et al. (2008), and this study).

influence from the Triassic-Jurassic boundary (~201 Ma) through the Early Cretaceous (~130 Ma), presumably as a result of gradually improving connectivity of the Neuquén Basin with the Panthalassic Ocean to its west (Fig. 8).

### 5.3. Fossils as salinity indicators

The primary evidence on which an interpretation of marine conditions for the AMF was based is the presence of putatively marine fossils (Fig. 7). However, the fossil content of the AMF has been described as low-diversity, sparse, and poorly preserved (Riccardi et al., 1997, 2004; Damborenea and Manceñido, 2012; Damborenea et al., 2017; Riccardi, 2019; Pérez Panera et al., 2023). Among the fossils recovered from this formation are small tests of agglutinated foraminifera (*Haplophragmoides*-like and nodosariids) and rare ostracods (*Ogmoconchella*) near the base of the section and around 250 m, all of which are poorly preserved (Riccardi et al., 1997). The most numerous macroinvertebrate clade is bivalves, of which at least 15 species are recognized, with specimens preserved mostly as external or internal molds in nodules (Riccardi et al., 2004; Damborenea and Manceñido, 2012; Damborenea et al., 2017). Both shallow infaunal and epifaunal suspension feeders are present, but one common species (*Asoella campbellorum* n. sp.) has a pendant habit, being associated with fragments of ammonite shells and driftwood debris (Damborenea and Manceñido, 2012). Other less common invertebrate clades include gastropods, ammonoids, cnidarians, brachiopods and nautiloids (Riccardi et al., 2004), and terrestrial plant remains include *Zuberia* cf. *zuberi* and other Equisetales (Riccardi et al., 1997, 2004).

Low and/or fluctuating salinities would have been a major environmental impediment to colonization of the latest Triassic Neuquén Basin by marine animals. Redox proxies ($Mo_{EF}$, $U_{EF}$, and $C_{org}/P$) are low enough to indicate that the AMF watermass was not markedly reducing (Fig. 5), which suggests that the impoverishment of the fossil biota was not related to low oxygen levels. The dominance of a single clade (i.e., bivalves) is consistent with reduced-salinity conditions (Whitfield et al., 2012). As a clade, bivalves exhibit relatively wide salinity tolerances (Pourmozaffar et al., 2020), and the relationship of specific bivalve taxa to salinity variation in the Neuquén Basin needs investigation. The presence of fossils of putative marine origin in the AMF is likely due to several processes. First, transportation of living or dead organisms from adjacent marine areas is common (Yacobucci, 2018). For example, modern *Nautilus* shells can float long distances before reaching their final sites of deposition (Reyment, 2008), which may account for the infrequent occurrence of ammonites as well as pendant bivalve species (Riccardi, 2019). Other transport processes such as storm surge and marine sediment reworking can be largely discounted owing to the low-energy environment in which the AMF was deposited. Second, some organisms regarded as stenohaline marine fauna have a wider salinity tolerance than commonly assumed (e.g., Bickert et al., 1997; Mángano et al., 2021). In this regard, elemental salinity proxies may prove useful for refining the salinity tolerances of various ancient taxonomic clades. Another possible explanation is the existance of strong salinity fluctuations around the opening of the Neuquén Basin to the Panthalassic Ocean, similar to those observed in the modern Baltic Sea, in which east–west wind conditions trigger episodic watermass exchange with the North Sea, allowing rapid but transient changes in salinity (Lehmann et al., 2022). In this case, the salinity record presented here for the Neuquén Basin would represent the freshwater endmember of a basin subject to strong lateral salinity gradients.

### 5.4. Timing of opening of the Neuquén Basin

Except for the Atuel depocenter, all subbasins of the Late Triassic Neuquén Basin were synrift grabens filled with continental, volcanic, and volcaniclastic deposits (Spalletti, 1997; Franzese et al., 2003; D'Elia et al., 2020). The closest and most similar one is the Malargüe-Llantenes depocenter, which contains lacustrine deposits of the Llantenes Formation (Tronquimalal Group) of probable Late Triassic age (Norian to? Rhaetian) (Spalletti, 1997; Morel et al., 2003). Its palynomorph assemblage includes *Linguifolium*, *Cupressaceae*, and *Protojuniperoxylon ischigualastense* (Artabe et al., 2001; Gnaedinger and Zavattieri, 2020), indicating a lake basin in a humid climatic belt, surrounded by deciduous forests and with the influence of marine incursions from the west (Gnaedinger and Zavattieri, 2020). Similar conditions are likely to have existed in the Late Triassic Neuquén Basin, accounting for the juxtaposition of marine fossils with elemental proxy evidence of low-salinity conditions. The strata overlying the AMF represent the earliest basin-scale marine inundation of the Neuquén Basin, which we date to the Pliensbachian (Early Jurassic).

## 6. Conclusions

Paleosalinity proxies (B/Ga, Sr/Ba, and S/TOC) demonstrate the existence of freshwater to weakly brackish conditions in the Neuquén Basin during the Triassic-Jurassic transition. These results contradict previous assumptions of marine salinities based on a poorly preserved

assemblage of putatively marine fossils of the Arroyo Malo Formation. Our results are more consistent with the Neuquén Basin being a large estuary that was weakly connected to the Panthalassic Ocean, subject to only occasional marine incursions. Thus, the AMF of the Atuel Depocenter represents a largely continental setting, similar to that of other Neuquén Basin depocenters during the Late Triassic. These findings demonstrate the importance of multiproxy approaches to establish paleosalinity conditions in continent-margin and marginal-marine basins and the need for application of paired salinity-redox proxies in order to correctly interpret paleoenvironmental variations.

## CRediT authorship contribution statement

**Mariano N. Remírez:** Conceptualization, Funding acquisition, Investigation, Methodology, Project administration, Validation, Visualization, Writing – original draft, Writing – review & editing. **Thomas J. Algeo:** Conceptualization, Data curation, Formal analysis, Investigation, Methodology, Resources, Visualization, Writing – original draft, Writing – review & editing. **Jun Shen:** Data curation, Formal analysis, Funding acquisition, Investigation, Resources. **Jinhua Liu:** Data curation, Formal analysis, Funding acquisition, Resources, Validation. **Geoffrey J. Gilleaudeau:** Conceptualization, Data curation, Formal analysis, Investigation, Methodology, Writing – original draft, Writing – review & editing. **Lian Zhou:** Data curation, Funding acquisition, Investigation, Resources, Validation.

## Declaration of competing interest

The authors declare the following financial interests/personal relationships which may be considered as potential competing interests:

Mariano Remirez reports financial support was provided by Fundación Williams.

## Data availability

I have attached an Excel file

## Acknowledgments

Thanks to Fundación Williams and SOMINAR S.A. for financial support to MR, and to Joaquín Orzanco and Tomás Navarro for field assistance. This research was partially supported by the Natural Science Foundation of China (92055201, 42072037), National Key Research and Development Program of China (2022YFF0803100), and the State Key Laboratory of Loess and Quaternary Geology (SKLLQGZR2207) to JS, 111 Project from National Bureau of Foreign Experts and the Ministry of Education of China (BP0820004) to JS. This work is a contribution to IGCP Project 739.

## Appendix A. Supplementary data

Supplementary data to this article can be found online at https://doi.org/10.1016/j.palaeo.2024.112216.

## References

Aguirre-Urreta, B., Lazo, D.G., Griffin, M., Vennari, V., Parras, A.M., Cataldo, C., Carbone, O., 2011. Megainvertebrados del Cretácico y su importancia bioestratigráfica. In: *Geología y Recursos Naturales de la Provincia del Neuquén*. Buenos Aires: Asociación Geológica Argentina, pp. 465–488.

Aguirre-Urreta, B., Martinez, M., Schmitz, M., Lescano, M., Omarini, J., Tunik, M., , et al. Pälike, H., 2019. Interhemispheric radio-astrochronological calibration of the time scales from the Andean and the Tethyan areas in the Valanginian–Hauterivian (Early Cretaceous). Gondwana Res. 70, 104–132.

Algeo, T.J., Ingall, E., 2007. Sedimentary $C_{org}$:P ratios, paleocean ventilation, and Phanerozoic atmospheric $pO_2$. Palaeogeogr. Palaeoclimatol. Palaeoecol. 256 (3–4), 130–155.

Algeo, T.J., Liu, J., 2020. A re-assessment of elemental proxies for paleoredox analysis. Chem. Geol. 540, 119549.

Anderson, T.F., Arthur, M.A., 1983. Stable isotopes of oxygen and carbon and their application to sedimentologic and paleoenvironmental problems. In: Arthur, M.A., Anderson, T.F. (Eds.), *Stable Isotopes in Sedimentary Geology*, SEPM Short Course, vol. 10. Society for Sedimentary Geology, Tulsa, 1.1-1.151.

Artabe, A.E., Morel, E.M., Spalletti, L.A., Brea, M., 1998. Paleoambientes sedimentarios y paleoflora asociada en el Triásico tardío de Malargüe, Mendoza. Rev. Asoc. Geol. Argent. 53 (4), 526–548.

Artabe, A.E., Morel, E.M., Spalletti, L.A., 2001. Paleoecología de las floras triásicas argentinas. In: Artabe, A.E., Morel, E.M., Zamuner, A.B. (Eds.), *El Sistema Triásico en la Argentina*. La Plata, Fundación Museo de La Plata "Francisco Pascasio Moreno,", pp. 199–225.

Bechis, F., Giambiagi, L.B., Tunik, M.A., Suriano, J., Lanés, S., Mescua, J.F., 2020. Tectono-stratigraphic evolution of the Atuel depocenter during the late Triassic to early Jurassic rift stage, Neuquén basin, west-Central Argentina. In: Kietzmann, D. (Ed.), Opening and Closure of the Neuquén Basin in the Southern Andes. Springer, pp. 23–52.

Bennett, W.W., Canfield, D.E., 2020. Redox-sensitive trace metals as paleoredox proxies: a review and analysis of data from modern sediments. Earth Sci. Rev. 204, 103175.

Berglund, B.E., Sandgren, P., Barnekow, L., Hannon, G., Jiang, H., Skog, G., Yu, S.Y., 2005. Early Holocene history of the Baltic Sea, as reflected in coastal sediments in Blekinge, southeastern Sweden. Quat. Int. 130 (1), 111–139.

Bhattacharya, J., 1978. Deltas and estuaries. In: Sedimentology. *Encyclopedia of Earth Science*. Springer, Berlin, Heidelberg. https://doi.org/10.1007/3-540-31079-7_62.

Bickert, T., Pätzold, J., Samtleben, C., Munnecke, A., 1997. Paleoenvironmental changes in the Silurian indicated by stable isotopes in brachiopod shells from Gotland, Sweden. Geochim. Cosmochim. Acta 61 (13), 2717–2730.

Breiter, K., Gardenová, N., Kanický, V., Vaculovic, T., 2013. Gallium and germanium geochemistry during magmatic fractionation and post-magmatic alteration in different types of granitoids: A case study from the Bohemian Massif (Czech Republic). Geol. Carpath. 64 (3), 171.

Cheng, M., Zhang, Z., Algeo, T.J., Liu, S., Liu, X., Wang, H., Chang, B., Jin, C., Pan, W., Cao, M., Li, C., 2021. Hydrological controls on marine chemistry in the Cryogenian Nanhua Basin (South China). Earth Sci. Rev. 218, 103678.

Chivas, A. R., García, A., van Der Kaars, S., Couapel, M. J., Holt, S., Reeves, J. M., … Cecil, C. B. (2001). Sea-level and environmental changes since the last interglacial in the Gulf of Carpentaria, Australia: an overview. Quat. Int., 83, 19–46.

Damborenea, S.E., Manceñido, M.Ó., 2012. Late Triassic bivalves and brachiopods from southern Mendoza, Argentina. Rev. Paléobiol. VS 11, 317–344.

Damborenea, S.E., Echevarría, J., Ros-Franch, S., 2017. Biotic recovery after the end-Triassic extinction event: evidence from marine bivalves of the Neuquén Basin, Argentina. Palaeogeogr. Palaeoclimatol. Palaeoecol. 487, 93–104.

D'Elia, L., Bilmes, A., Naipauer, M., Vergani, G.D., Muravchik, M., Franzese, J.R., 2020. The syn-rift of the Neuquén Basin (Precuyano and Lower Cuyano cycle): Review of structure, volcanism, tectono-stratigraphy and depositional scenarios. In: Kietzmann, D. (Ed.), Opening and Closure of the Neuquén Basin in the Southern Andes. Springer, pp. 3–21.

Deyhle, A., Kopf, A.J., 2005. The use and usefulness of boron isotopes in natural silicate–water systems. Phys Chem Earth, Parts A/B/C 30 (17–18), 1038–1046.

Donahoe, R.J., Liu, C., 1998. Pore water geochemistry near the sediment-water interface of a zoned, freshwater wetland in the southeastern United States. Environ. Geol. 33, 143–153.

Dymond, J., Suess, E., Lyle, M., 1992. Barium in deep-sea sediment: A geochemical proxy for paleoproductivity. Paleoceanography 7 (2), 163–181.

Echevarría, J., Hodges, M.S., Damborenea Jr., S.E., G. D. S., and Manceñido, M. O., 2017. Recovery of scleractinian morphologic diversity during the Early Jurassic in Mendoza Province, Argentina. Ameghiniana 54 (1), 70–82.

Feldman, M.D., Kwon, S.T., Boles, J.R., Tilton, G.R., 1993. Diagenetic mass transport in the southern San Joaquin basin, California, USA: Implications from the strontium isotopic composition of modern pore fluids. Chem. Geol. 110 (4), 329–343.

Foley, N.K., Jaskula, B.W., Kimball, B.E., Schulte, R.F., 2017. Gallium. In: Schulz, K.J., DeYoung Jr., J.H., Seal II, R.R., Bradley, D.C. (Eds.), Critical Mineral Resources of the United States—Economic and Environmental Geology and Prospects for Future Supply, 1802. U.S. Geol. Survey Prof. Pap, pp. H1–H35. https://doi.org/10.3133/pp1802H.

Franzese, J., Spalletti, L., Pérez, I.G., Macdonald, D., 2003. Tectonic and paleoenvironmental evolution of Mesozoic sedimentary basins along the Andean foothills of Argentina (32–54 S). J. S. Am. Earth Sci. 16 (1), 81–90.

Fürsich, F.T., 1994. Palaeoecology and evolution of Mesozoic salinity-controlled benthic macroinvertebrate associations. Lethaia 26 (4), 327–346.

Gasparini, Z., Fernández, M., 2005. Jurassic marine reptiles of the Neuquén Basin: records, faunas and their palaeobiogeographic significance. Geol. Soc. Lond. Spec. Publ. 252 (1), 279–294.

Gilleaudeau, G.J., Wei, W., Remírez, M.N., Song, Y., Lyons, T.W., Bates, S., Algeo, T.J., 2023. Geochemical and hydrographic evolution of the late Devonian Appalachian Seaway: linking sedimentation, redox, and salinity across time and space. Geochem. Geophys. Geosyst. 24 (8) e2023GC010973.

Gnaedinger, S.C., Zavattieri, A.M., 2020. Coniferous woods from the Upper Triassic of southwestern Gondwana, Tronquimalal Group, Neuquén Basin, Mendoza Province, Argentina. J Paleontol. 94 (3), 387–416.

Hanebuth, T.J., Proske, U., Saito, Y., Nguyen, V.L., Ta, T.K.O., 2012. Early growth stage of a large delta—Transformation from estuarine-platform to deltaic-progradational conditions (the northeastern Mekong River Delta, Vietnam). Sediment. Geol. 261, 108–119.

Hassanzadeh, S., Hosseinibalam, F., Rezaei-Latifi, A., 2011. Numerical modelling of salinity variations due to wind and thermohaline forcing in the Persian Gulf. Appl. Math. Model. 35 (3), 1512–1537.

Holland, H.D., Turekian, K.K., 2010. *Geochemistry of Earth Surface Systems*: A Derivative of the Treatise on Geochemistry. Academic Press.
Howell, J.A., Schwarz, E., Spalletti, L.A., Veiga, G.D., 2005. The Neuquén basin: An overview. In: Veiga, G., Spalletti, L., Howell, J., Schwarz, E. (Eds.), The Neuquén Basin: A Case Study in Sequence Stratigraphy and Basin Dynamics, Geological Society of London, Special Publication, vol. 252, pp. 1–14.
Keren, R., Mezuman, U., 1981. Boron adsorption by clay minerals using a phenomenological equation. Clay Clay Miner. 29, 198–204.
Lanés, S., 2002. Paleoambientes y Paleogeografía de la primera transgresión en Cuenca Neuquina, Sur de Mendoza. Ph.D. thesis. Universidad de Buenos Aires, Argentina, p. 403.
Lanés, S., 2005. Late Triassic to early Jurassic sedimentation in northern Neuquén Basin, Argentina: tectosedimentary evolution of the first transgression. Geol. Acta 3 (2), 81–106.
Lanés, S., Giambiagi, L., Bechis, F., Tunik, M., 2008. Late Triassic-early Jurassic successions of the Atuel depocenter: sequence stratigraphy and tectonic controls. Rev. Asoc. Geol. Argent. 63 (4), 534–548.
Lazo, D.G., Cichowolski, M., Rodríguez, D.L., Aguirre-Urreta, M.B., 2005. Lithofacies, palaeoecology and palaeoenvironments of the Agrio Formation, lower cretaceous of the Neuquén Basin, Argentina. In: Veiga, G., Spalletti, L., Howell, J., Schwarz, E. (Eds.), The Neuquén Basin: A Case Study in Sequence Stratigraphy and Basin Dynamics, vol. 252. Geological Society of London, Special Publication, pp. 295–315.
Lazo, D.G., Aguirre-Urreta, M.B., Price, G.D., Rawson, P.F., Ruffell, A.H., Ogle, N., 2008. Palaeosalinity variations in the early cretaceous of the Neuquén Basin, Argentina: evidence from oxygen isotopes and palaeoecological analysis. Palaeogeogr. Palaeoclimatol. Palaeoecol. 260 (3–4), 477–493.
Lehmann, A., Myrberg, K., Post, P., Chubarenko, I., Dailidiene, I., Hinrichsen, H.H., Hüsy, K., Liblik, T., Mayer, H.E.M., Lips, U., Bukanova, T., 2022. Salinity dynamics of the Baltic Sea. Earth Syst. Dynam. 13 (1), 373–392.
Liu, Z., Algeo, T.J., Arefifard, S., Wei, W., Brett, C., Landing, E., Lev, S.M., 2024. Testing the salinity of Cambrian to Silurian epicratonic seas. J. Geol. Soc. jgs2023–217.
Machel, H.G., 2001. Bacterial and thermochemical sulfate reduction in diagenetic settings-old and new insights. Sediment. Geol. 140 (1–2), 143–175.
Mackin, J.E., 1987. Boron and silica behavior in salt-marsh sediments; implications for paleo-boron distributions and the early diagenesis of silica. Am. J. Sci. 287 (3), 197–241.
Manceñido, M.Ó., Damborene, S.E., 2005. Biofacies analysis of Hettangian-Sinemurian bivalve/brachiopod associations from the Neuquén Basin (Argentina). Geol. Acta 163–178.
Mángano, M.G., Buatois, L.A., Waisfeld, B.G., Muñoz, D.F., Vaccari, N.E., Astini, R.A., 2021. Were all trilobites fully marine? Trilobite expansion into brackish water during the early Palaeozoic. Proc. R. Soc. B 288 (1944), 20202263.
Marin, L.S., Aguirre-Urreta, B., Rawson, P.F., 2023. Lower cretaceous ammonoids from the Neuquén Basin, Argentina: the late Hauterivian *Paraspiticeras* and associated faunas. Cretac. Res. 145, 105478.
Martínez, M.A., Prámparo, M.B., Quattrocchio, M.E., Zavala, C.A., 2008. Depositional environments and hydrocarbon potential of the Middle Jurassic Los Molles Formation, Neuquén Basin, Argentina: palynofacies and organic geochemical data. Andean Geol. 35 (2), 279–305.
Millero, F.J., Feistel, R., Wright, D.G., McDougall, T.J., 2008. The composition of Standard Seawater and the definition of the Reference-Composition Salinity Scale. Deep Sea Res. Part 1 Oceanogr. Res. Pap. 55 (1), 50–72.
Moore, S.A., Birgenheier, L.P., Greb, M.D., Minisini, D., Tunik, M., Omarini, J., 2020. Integrated depositional model and hydrocarbon potential of distal ramp deposits, Agrio Formation, Neuquén Basin, Argentina. J. Sediment. Res. 90 (5), 533–570.
Morel, E.M., Artabe, A.E., Spalletti, L.A., 2003. Triassic floras of Argentina: biostratigraphy, floristic events and comparison with other areas of Gondwana and Laurasia. Alcheringa 27 (3), 231–243.
Mpodozis, C., Ramos, V., 1990. The Andes of Chile and Argentina. In: Ericksen, G.E., Canas Pinochet, M.T., Reinemund, J.A. (Eds.), Geology of the Andes and its Relation to Hydrocarbon and Mineral Resources, vol. v. 11. Circum-Pacific Council for Energy and Mineral Resources Earth Science Series, Houston, Texas, pp. 59–73.
Muttik, N., Kirsimäe, K., Newsom, H.E., Williams, L.B., 2011. Boron isotope composition of secondary smectite in suevites at the Ries crater, Germany: boron fractionation in weathering and hydrothermal processes. Earth Planet. Sci. Lett. 310 (3–4), 244–251.
Nali, M., Caccialanza, G., Ghiselli, C., Chiaramonte, M.A., 2000. $T_{max}$ of asphaltenes: a parameter for oil maturity assessment. Org. Geochem. 31 (12), 1325–1332.
Olivera, D.E., Martínez, M.A., Zavala, C., Di Nardo, J.E., Otharán, G., 2020. New contributions to the palaeoenvironmental framework of the Los Molles Formation (Early-to-Middle Jurassic), Neuquén Basin, based on palynological data. Facies 66 (4), 1–21.
Panahi, A., Young, G.M., Rainbird, R.H., 2000. Behavior of major and trace elements (including REE) during Paleoproterozoic pedogenesis and diagenetic alteration of an Archean granite near Ville Marie, Québec, Canada. Geochim. Cosmochim. Acta 64 (13), 2199–2220.
Panera, J.P.P., Angelozzi, G.N., Riccardi, A.C., Damborenea, S.E., Manceñido, M.O., 2023. Late Triassic Calcareous Nannofossils from Arroyo Malo Formation, Neuquén Basin, Argentina. Implications for their early Evolution and Dispersal. Ameghiniana 60 (2), 149–163.
Percival, L.M., Ruhl, M., Hesselbo, S.P., Jenkyns, H.C., Mather, T.A., Whiteside, J.H., 2017. Mercury evidence for pulsed volcanism during the end-Triassic mass extinction. In: Proceedings of the National Academy of Sciences (U.S.A.), 114(30), pp. 7929–7934.
Perry, E.A., 1972. Diagenesis and the validity of the boron paleosalinity technique. Am. J. Sci. 272 (2), 150–160.
Pourmozaffar, S., Tamadoni Jahromi, S., Rameshi, H., Sadeghi, A., Bagheri, T., Behzadi, S., Gozari, M., Zahedi, M.R., Abrari Lazarjani, S., 2020. The role of salinity in physiological responses of bivalves. Rev. Aquac. 12 (3), 1548–1566.
Pritchard, D.W., 1952. Salinity distribution and circulation in the Chesapeake Bay estuarine system. J. Mar. Res. 11, 106–123.
Redfield, A.C., 1963. The influence of organisms on the composition of seawater. *The Sea, vol. 2*, Interscience Publishers, New York, pp. 26-77.
Privat, A.M.L., Hodgson, D.M., Jackson, C.A.L., Schwarz, E., Peakall, J., 2021. Evolution from syn-rift carbonates to early post-rift deep-marine intraslope lobes: the role of rift basin physiography on sedimentation patterns. Sedimentology 68 (6), 2563–2605.
Reeves, J.M., Chivas, A.R., García, A., Holt, S., Couapel, M.J., Jones, B.G., Fink, D., 2008. The sedimentary record of palaeoenvironments and sea-level change in the Gulf of Carpentaria, Australia, through the last glacial cycle. Quat. Int. 183 (1), 3–22.
Remírez, M.N., Algeo, T.J., 2020. Paleosalinity determination in ancient epicontinental seas: A case study of the T-OAE in the Cleveland Basin (UK). Earth Sci. Rev. 201, 103072.
Remírez, M.N., Dacal, A.G., Orzanco, J., 2022a. Controls on the accumulation of early cretaceous organic-rich fine-grained deposits in a mixed marine siliciclastic-carbonate distal settings of the Neuquén Basin, Central-Western Argentina. Mar. Pet. Geol. 146, 105962.
Remírez, M.N., Spalletti, L.A., Isla, M.F., Schwarz, E., 2022b. Fine-grained distal deposits of a mixed siliciclastic–carbonate marine system: Origin of mud and implications on mixing processes. J. Sediment. Res. 92 (3), 210–231.
Reyment, R.A., 2008. A review of the post-mortem dispersal of cephalopod shells. Palaeontol. Electron. 11 (3), 1–13.
Reynolds, R.M., 1993. Physical oceanography of the Gulf, Strait of Hormuz, and the Gulf of Oman—Results from the Mt. Mitchell expedition. Mar. Pollut. Bull. 27, 35–59.
Riccardi, A.C., 2019. Cephalopods from the Triassic-Jurassic boundary interval in west Central Argentina. Neues Jahrbuch für Geologie und Paläontologie-Abhandlungen 291, 135–157.
Riccardi, A.C., Iglesia Llanos, M.P., 1999. Primer hallazgo de amonites en el Triásico de la Argentina. Rev. Asoc. Geol. Argent. 54 (3), 298–300.
Riccardi, A.C., Damborenea, S.E., Manceñido, M.O., Ballent, S.C., 1991. Hettangian and Sinemurian (lower Jurassic) biostratigraphy of Argentina. J. S. Am. Earth Sci. 4 (3), 159–170.
Riccardi, A.C., Damborenea, S.E., Manceñido, M.O., Scasso, R., Lanés, S., Iglesia Llanos, M.P., Stipanicic, P.N., 1997. Primer registro de Triásico marino fosilífero de la Argentina. Rev. Asoc. Geol. Argent. 52 (2), 228–234.
Riccardi, A.C., Damborenea, S.E., Manceñido, M.O., Ballent, S.C., 1999. El Jurásico y Cretácico de la Cordillera Principal y la cuenca Neuquina. In: Eduardo, O., et al. (Eds.), Zappettini. Recursos Minerales de la República Argentina, pp. 419–432.
Riccardi, A.C., Damborenea, S.E., Manceñido, M.O., Iglesias Llanos, M.P., 2004. The Triassic/Jurassic boundary in the Andes of Argentina. Riv. Ital. Paleontol. Stratigr. 110 (1), 69–76.
Riccardi, A.C., Damborenea, S.E., Manceñido, M.O., Leanza, H.A., 2011. Megainvertebrados del Jurásico y su importancia geobiológica. In: Relatorio XVIII Congreso Geológico Argentino. Neuquén, Argentina, pp. 441–464.
Ruhl, M., Hesselbo, S.P., Al-Suwaidi, A., Jenkyns, H.C., Damborenea, S.E., Manceñido, M.O., Storm, M., Mather, T.A., Riccardi, A.C., 2020. On the onset of Central Atlantic Magmatic Province (CAMP) volcanism and environmental and carbon-cycle change at the Triassic–Jurassic transition (Neuquén Basin, Argentina). Earth Sci. Rev. 208, 103229.
Rytuba, J.J., John, D.A., Foster, A., Ludington, S.D., Kotlyar, B., 2003. Hydrothermal enrichment of gallium in zones of advanced argillic alteration—examples from the Paradise Peak and McDermitt ore deposits, Nevada. In: Bliss, James D., Moyle, Phillip R., Long, Keith R. (Eds.), Contributions to Industrial-Minerals Research. U.S. Geol. Surv. Bull. 2209-C, p. 16.
Salminen, R., et al., 2005. *Geochemical Atlas of Europe*. Part 1: Background Information, Methodology and Maps. Geological Survey of Finland, Espoo, Finland downloaded at 17.12.2006. http://www.gtk.fi/publ/foregsatlas.
Schwarz, E., Remírez, M., Lazo, D.G., Veiga, G.D., Isla, M.I., Echevarria, C., Toscano, A., Garberoglio, R.M., 2022. A review on depositional systems, bioevents and paleogeography of the Valanginian-Hauterivian Neuquén Sea: refining sedimentary and biological signals linked to the dynamics of epeiric seas. Earth Sci. Rev. 234, 104224.
Shiller, A.M., Frilot, D.M., 1996. The geochemistry of gallium relative to aluminum in Californian streams. Geochim. Cosmochim. Acta 60 (8), 1323–1328.
Somers, I.F., Long, B.G., 1994. Note on the sediments and hydrology of the Gulf of Carpentaria, Australia. Mar. Freshw. Res. 45 (3), 283–291.
Song, Y., Gilleaudeau, G.J., Algeo, T.J., Over, D.J., Lyons, T.W., Anbar, A.D., Xie, S., 2021. Biomarker evidence of algal-microbial community changes linked to redox and salinity variation, Upper Devonian Chattanooga Shale (Tennessee, USA). GSA Bull. 133 (1–2), 409–424.
Spalletti, L.A., 1997. Sistemas deposicionales fluvio-lacustres en el rift triásico de Malargüe (sur de Mendoza, República Argentina). Anales de la Academia Nacional de Ciencias Exactas, Físicas y Naturales 49, 109–124.
Spalletti, L.A., Parent, H., Veiga, G.D., Schwarz, E., 2012. Amonites y Bioestratigrafía del grupo Cuyo en la Sierra de Reyes (Cuenca Neuquina central, Argentina) y su significado secuencial. Andean Geol. 39 (3), 464–481.
Spivack, A.J., Edmond, J.M., 1987. Boron isotope exchange between seawater and the oceanic crust. Geochim. Cosmochim. Acta 51 (5), 1033–1043.
Środoń, J., Paszkowski, M., 2011. Role of clays in the diagenetic history of nitrogen and boron in the Carboniferous of Donbas (Ukraine). Clay Miner. 46 (4), 561–582.

Sullivan, M.D., Haszeldine, R.S., Fallick, A.E., 1990. Linear coupling of carbon and strontium isotopes in Rotliegend Sandstone, North Sea: evidence for cross-formational fluid flow. Geology 18 (12), 1215–1218.
Tribovillard, N., Algeo, T.J., Lyons, T., Riboulleau, A., 2006. Trace metals as paleoredox and paleoproductivity proxies: an update. Chem. Geol. 232 (1–2), 12–32.
Tyson, R.V., 2012. Sedimentary Organic Matter: Organic Facies and Palynofacies. Springer, Berlin.
Vergani, G.D., Tankard, A.J., Belotti, H.J., Welsink, H.J., 1995. Tectonic evolution and paleogeography of the Neuquén Basin, Argentina. In: Tankard, A.J., Suárez, R., Soruco, R., Welsink, H.J. (Eds.), Petroleum Basins of South America, American Association of Petroleum Geologists, Memoir, vol. 62, pp. 383–402.
Villumsen, A., Nielsen, O.B., 1976. The influence of palaeosalinity, grain size distribution and clay minerals on the content of B, Li and Rb in Quaternary sediments from Eastern Jutland, Denmark. Sedimentology 23 (6), 845–855.
Voipio, A., 1981. The Baltic Sea. Elsevier Oceanography Series, Amsterdam, p. 30.
Wang, W., Qin, Y., Liu, X., Zhao, J., Wang, J., Wu, G., Liu, J., 2011. Distribution, occurrence and enrichment causes of gallium in coals from the Jungar Coalfield, Inner Mongolia. Sci. China Earth Sci. 54, 1053–1068.
Watanabe, Y., Farquhar, J., Ohmoto, H., 2009. Anomalous fractionations of sulfur isotopes during thermochemical sulfate reduction. Science 324 (5925), 370–373.
Weckström, K., Lewis, J.P., Andrén, E., Ellegaard, M., Rasmussen, P., Ryves, D.B., Telford, R., 2017. Palaeoenvironmental history of the Baltic Sea: One of the largest Brackish-water ecosystems in the world. In: Weckström, K., Saunders, K.M., Gell, P. A., Skilbeck, C.G. (Eds.), Applications of Paleoenvironmental Techniques in Estuarine Studies. Springer, Berlin, pp. 615–662.
Wedepohl, K.H., 1991. The composition of the upper Earth's crust and the natural cycles of selected metals. In: Merian, E. (Ed.), Metals and their Compounds in the Environment. VCH-Verlagsgesellschaft, Weinheim, pp. 3–17.
Wei, W., Algeo, T.J., 2020. Elemental proxies for paleosalinity analysis of ancient shales and mudrocks. Geochim. Cosmochim. Acta 287, 341–366.
Wei, W., Yu, W., Algeo, T.J., Herrmann, A.D., Zhou, L., Liu, J., Wang, Q., Du, Y., 2022. Boron proxies record paleosalinity variation in the north American Midcontinent Sea in response to Carboniferous glacio-eustasy. Geology 50 (5), 537–541.
Whitfield, A.K., Elliott, M., Basset, A., Blaber, S.J.M., West, R.J., 2012. Paradigms in estuarine ecology–a review of the Remane diagram with a suggested revised model for estuaries. Estuar. Coast. Shelf Sci. 97, 78–90.
Williams, L.B., Hervig, R.L., 2002. Intracrystalline boron isotope variations in clay minerals: a potential low-temperature single mineral geothermometer. Am. Mineral. 87, 1564–1570.
Williams, L.B., Hervig, R.L., 2005. Lithium and boron isotopes in illite-smectite: the importance of crystal size. Geochim. Cosmochim. Acta 69 (24), 5705–5716.
Williams, L.B., Hervig, R.L., Holloway, J.R., Hutcheon, I., 2001. Boron isotope geochemistry during diagenesis. Part I. Experimental determination of fractionation during illitization of smectite. Geochim. Cosmochim. Acta 65 (11), 1769–1782.
Williams, L.B., Turner, A., Hervig, R.L., 2007. Intracrystalline boron isotope partitioning in illite-smectite: Testing the geothermometer. Am. Mineral. 92 (11−12), 1958–1965.
Yacobucci, M.M., 2018. Postmortem transport in fossil and modern shelled cephalopods. PeerJ 6, e5909.
Yang, S., Horsfield, B., 2020. Critical review of the uncertainty of $T_{max}$ in revealing the thermal maturity of organic matter in sedimentary rocks. Int. J. Coal Geol. 225, 103500.
Yang, S.Y., Li, C.X., Yang, D.Y., Li, X.S., 2004a. Chemical weathering of the loess deposits in the lower Changjiang Valley, China, and paleoclimatic implications. Quat. Int. 117 (1), 27–34.
Yang, S.Y., Jung, H.S., Li, C., 2004b. Two unique weathering regimes in the Changjiang and Huanghe drainage Basins: geochemical evidence from river sediments. Sediment. Geol. 164 (1), 19–34.
Yang, S.Y., Li, C., Cai, J., 2006. Geochemical compositions of core sediments in eastern China: implication for late Cenozoic palaeoenvironmental changes. Palaeogeogr. Palaeoclimatol. Palaeoecol. 229 (4), 287–302.
You, C.F., Spivack, A.J., Gieskes, J.M., Martin, J.B., Davisson, M.L., 1996. Boron contents and isotopic compositions in pore waters: a new approach to determine temperature induced artifacts—geochemical implications. Mar. Geol. 129 (3–4), 351–361.
Zapata, T., Folguera, A., 2005. Tectonic evolution of the Andean fold and thrust belt of the southern Neuquén Basin, Argentina. In: Veiga, G., Spalletti, L., Howell, J., Schwarz, E. (Eds.), The Neuquén Basin: A Case Study in Sequence Stratigraphy and Basin Dynamics, Geological Society of London, Special Publication, vol. 252, pp. 37–56.